ARTICLE

Understanding the photocatalytic properties of the Pt/CeOx/TiO_2 systems: structural effects on the electronic and optic properties

Jose J. Plata,[a]* Elena R. Remesal, [a] Jesús Graciani, [a] Antonio M. Márquez, [a] José A. Rodríguez, [b] and Javier Fernández Sanz[a]*

Abstract: Ceria-titania interfaces play a crucial role in different chemical processes but are especially promising for the photocatalytic splitting of water in the visible region when Pt is added to the system. However, the complexity of this hierarchical structures hampers the study of the origin of their outstanding properties. In this article, the structural, electronic and optoelectronic properties of CeO_2/TiO_2 systems containing 1D, 2D, and 3D particles of ceria are analyzed by means of density functional calculations. Adsorption sites and vacancies effects have been studied to model Pt adsorption. Density of states calculations and absorption spectra simulations explain the behavior of these systems. Finally, these models are used for the screening of other metals that can be combined with this heterostructure to potentially find more efficient water splitting photocatalysts.

Introduction

The reducibility of TiO_2 and CeO_2 makes these oxides suitable for a wide range of applications, especially in catalysis.[1, -4] They can be used as supports for metal nanoparticles, usually in oxidation or reduction processes,[5, 6, 7] or for absorbing photons in photocatalytic reactions.[8, 9] Although there are many studies demonstrating the activity of these two oxides individually, recent reports have pointed out the benefits of combining ceria and titania.[10, 11] Solid solutions of these two oxides can be synthesized with different structures depending on the content of each cation. While anatase is the predominant structural feature when the Ce content is below 10%, fluorite-like structures are formed when the Ti amount is lower than 30%.[10] This solid solution has shown promising results for different reactions such as NH_3 oxidation,[10] desulfurization applications,[12] water-gas shift (WGS) reaction [13] and photo degradation of organic molecules. [14]

Ceria-titania systems go beyond the formation of solid solutions. In the literature, heterostructures combining these two oxides have become common in the past five years. TiO_2 clusters on CeO_2 (111) reduce the vacancy formation energy and enhances the oxidation power of this catalytic substrate.[15] However, it is the inverse configuration, CeO_2 on TiO_2, which has attracted more attention. Nanoparticles of ceria on a rutile TiO_2(110) single crystal or on anatase powders exhibit unique structural and electronic properties not seen for bulk ceria.[16 -19] Size effects and a strong oxide-oxide interaction are responsible for this phenomenon.[16 - 19] In this aspect, a ceria-titania interface presents an exceptional activity for the dehydrogenation of methanol to formaldehyde at very low temperatures[20] or water-gas shift reaction if Pt is adsorbed on the surface.[21]

Among all potential applications for this system, photocatalysis stands as the most promising. Ceria nanostructures (e.g. nanocomposites or nanotubes) on TiO_2 are widely applied to catalyse the reduction of nitro compounds,[22] the photoreduction of CO_2 to methanol[23 24] and methane[24] degradation of organic contaminant[25, 26, 27] or microorganism elimination.[28] The photo-catalytic behaviour of the system seems to be strongly correlated to two factors: i) the interface between the two oxides.[25, 29, 30] and ii) metals adsorption on its surface.[16] Near Edge X-Ray Absorption Fine Structure (NEXAFS) and UV-vis measurements have proved that the deposition of CeO_x nanoparticles on TiO_2 is an efficient way to modify the chemical and electronic properties of both oxides.[16] The authors of this work suggested the preferential presence of Ce^{3+} cations at the interface, which creates mid gap states which absorb photons in the visible region. These findings have been confirmed by DFT calculations.[17] Furthermore, it was found that the growth of the ceria is influenced by the strain originated by the lattice mismatch between ceria and titania. High-angle annular dark-field scanning transmission electron microscopy (HAADF STEM) imaging demonstrates that ceria exists in a hierarchical structure with clusters, chains, and nanoparticles in samples with increasing ceria loadings ranging from 1 to 6 wt % on the titania support.[17, 18]

The photoactivity of these hierarchical structures can also be modified by the adsorption of metal nanoparticles. The nanostructures of ceria dispersed on titania seem to have a stronger interaction with metals than seen in the case of bulk ceria.[16 - 19] It has been reported that Au/TiO_2-CeO_2 catalyst actively photo-oxidizes 2-propanol.[31] Ni has also been used on these mixed-oxide systems for CO_2 methanation.[32] However, Pt is the most adsorbed noble metal on CeO_2-TiO_2 nanostructures as photocatalyst.[16,17,33] For instance, when compared to plain TiO_2 or Pt/TiO_2, Pt/CeO_x/TiO_2, seems to be promising for the photocatalytic splitting of water in the visible region.[17] However, it is still unclear how metals modify the electronic properties of this system and enhances its photocatalytic performance.[16]

In this article, we analyze the interaction of Pt atoms with well-characterized CeO_x/TiO_2 nanostructures. The impact of the Pt adsorption on the electronic structure are examined in detail and their effects in the absorption spectra are rationalized to understand the photocatalytic properties of the system. These results are used later to perform a systematic study in which Pt is substituted by other metals to accelerate the prediction of systems with potentially similar or higher activity.

[a] Dr. J. J. Plata, E. R. Remesal, Prof. Dr. J. Graciani, Prof. Dr. A. M. Márquez, and Prof. Dr. J. Fernández Sanz
Department: Departamento de Química Física, Facultad de Química
Institution: Universidad de Sevilla
Address 1: Profesor García González, s/n 41012 Sevilla
E-mail: jplata@us.es, sanz@us.es.

[b] Dr. J. A. Rodríguez
Department: Chemistry Department
Institution Brookhaven National Laboratory
Address 2: Upton, New York 11973-5000, United States

Results and Discussion

Pt adsorption. To the best of our knowledge, there are no studies of Pt adsorption on these hierarchical structures in which an interface with TiO_2 significantly changes the properties of the system compared to CeO_2 clean surfaces[34,35], or clusters.[36] To this end, we adsorbed single Pt atoms on all 3D, 2D, and 1D ceria nanostructures (Figure 1 and Figure S1-S3) which have been built using HAADF STEM images.[17] The adsorption energies of Pt on the 3D nanocluster are included in Table 1 and the adsorption sites are depicted in Figure 1e. Adsorption energies on the 3D cluster facets, exposing the CeO_2 (110) surface, range between -2.36 and -2.73 eV which are closer to values reported for CeO_2 (110) clean surfaces (-2.62 to -2.80 eV).[37] The CeO_2/TiO_2 interface sites present higher adsorption energies (-2.60 to -3.27 eV) than those of the facets. Although these values cannot be directly compared to those obtained for CeO_2 (111) steps (-5.0 to -6.7 eV), [38] both, the CeO_2/TiO_2 interface and steps act as preferential adsorption sites compared to the CeO_2 cluster facets or the clean TiO_2 surface. The adsorption of the Pt at the top of the nanoparticle presents the highest adsorption energy for this structure (-4.89 eV). This is very close to the -5.16 eV value reported for the (100) surface[37] with a very similar atomic arrangement. This adsorption energy is similar to the values obtained for the 2D model where the Pt is adsorbed on top oft he Ceria layer (Figure S4). No significant changes were found in the adsorption energies for the 2D model when 2 (-5.23 eV) or 5 (-5.28 eV) layers of CeO_2 were used and they are very close to the values reported for the clean (100) CeO_2 surface (-5.16 eV). [37] Pt was also adsorbed on the TiO_2 (112) surface to elucidate its preference for one or the other oxide obtaining, in this case, an adsorption energy of -2.80 eV. This value is higher than other obtained at the 3D cluster facets but considerably lower than those of sites close to the interface or the corner. Adsorption energies at the interface or in the 1D CeO_2 monomer (-2.7 eV) are closer to the values obtained for the TiO_2 surface than E_{ads} obtained for the (100) CeO_2 surface.

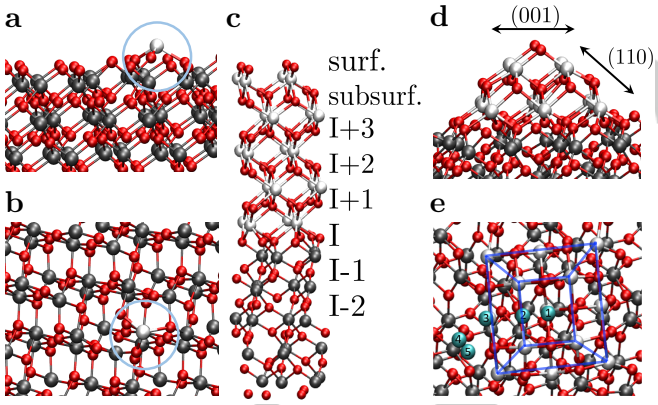

Figure 1. (a) and (b) Monomer (1D) CeO_2 cluster on TiO_2 (112) surface. (c) Interface (2D) model between CeO_2 (100) and TiO_2 (112) surfaces. (d) and (e) Pyramidal (3D) CeO_2 (100) cluster on top of TiO_2 (112) surface. CeO_2 monomer is highlighted in a blue circle in (a) and (b). I+x, surf. and subsurf. labels indicate the different oxygen layers where vacancies can be created. The Pt adsorption sites are included in (d): 1= corner; 2, 3 = facet; 4, 5= interface. Atom colors: Ce = white, Pt = cyan, O = red, Ti = grey.

Table 1. Pt adsorption energies, E_{ads}, for the 1D, 2D, and 3D CeO_2 hierarchical structures and TiO_2 (112) surface. E_{ads} in eV.

Model	Site	E_{ads}
3D	Corner	-4.89
	Facet	-2.36-2.73
	Interface	-2.60-3.27
2D	-	-5.23
1D	-	-2.7
TiO_2 (112)	-	-2.80

Pt and oxygen vacancies interaction. Vacancies and Ce^{3+} can modify the interaction between the Pt atoms and the surface. In order to evaluate the influence of vacancies on Pt adsorption, Pt atoms were adsorbed on 2D models with 2 CeO_2 layers and with vacancies at different positions (Table 2). Vacancy formation energy, E_V, is calculated as: $E_V = E_{CeO(2-x)/TiO2} + 0.5E_{O2} - E_{CeO2/TiO2}$, where $E_{CeO2/TiO2}$ and $E_{CeO(2-x)/TiO2}$ are the DFT energies obtained for the stoichiometric and non-stoichiometric (one oxygen vacancy) respectively. Similarly, the variation on the Pt adsorption energy when in the presence of vacancies, ΔE_{ads}, and the variation of vacancy formation energy with a Pt atom adsorbed with respect the clean surface, ΔE_V, are defined as:

$$\Delta E_{ads} = E_{ads}(Vac) - E_{ads}$$

$$\Delta E_V = E_V(Pt) - E_V$$

where Pt and Vac labels indicate whether adsorption energies or vacancy formation energies are calculated on a system with a Pt atom or a vacancy respectively.

Table 2. Pt adsorption energies with vacancies, $E_{ads}(Vac)$; variation of Pt adsorption energies with vacancies with respect to the stoichiometric system, ΔE_{ads}, vacancy formation energy with a Pt atom adsorbed, $E_V(Pt)$, and variation of vacancy formation energy with a Pt atom adsorbed with respect the clean surface, ΔE_V at different vacancy positions in the 2D model. E_{ads}, ΔE_{ads}, E_V, and ΔE_V in eV.

Position	$E_{ads}(Vac)$	ΔE_{ads}	$E_V(Pt)$	ΔE_V
Surface	-3.93	1.3	3.67	1.32
Subsurface	-4.68	0.55	2.94	0.57
Interface	-5.1	0.13	2.95	0.16
I-1	-4.94	0.29	3.11	0.30
I-2	-5.31	-0.08	3.93	-0.06

The data shown on Table 2 indicate that oxygen vacancy formation reduces the Pt adsorption energies compared to the stoichiometric system regardless of the vacancy position. This trend is more important when the vacancy is close to the Pt atom either at the surface or subsurface, reducing the Pt adsorption energy, ΔE_{ads}, between 1.3 eV and 0.55 eV. However, this effect is moderate when the vacancy is at the interface or in the TiO_2 phase (I-1 and I-2 sites). The vacancy formation energy is also modified when Pt is adsorbed. While there are not important modifications in the vacancy formation energy at the interface or the TiO_2 phase with respect to the clean surface, surface and subsurface vacancies are clearly destabilized by the Pt adsorption around 1.32 eV and 0.57 eV respectively. A similar trend, was reported by Vayssilov et *al* in Pt cluster on CeO_2 nanoparticles.[39] They found that the vacancy formation energy,

E_V, in ceria increases because of the adsorption of Pt and it is only reduced if there is an oxygen reverse spillover on the Pt nanocluster. This effect stems from the overreduction of the ceria phase where each vacancy reduces the ceria phase creating two Ce^{3+} polarons and the Pt atoms also donate electron density to the surface.[37] That is why, the trend is attenuated if the vacancy and the Pt are not close to each other.

Electronic structure. Understanding the electronic properties of these hierarchical structures is a first step to explain their photocatalytic behaviour. Density of states, DOS, for the 2D system with vacancies, CeO_x/TiO_2, with adsorbed Pt atoms, $Pt/CeO_2/TiO_2$ and with Pt and vacancies, $Pt/CeO_x/TiO_2$ are shown in Figure 2. There are common features in all cases: i) the valence band is mainly constituted by the O 2*p* states of both oxides, ii) the bottom edge of the conduction band corresponds to the Ce 4*f* band and iii) the Ti 3*d* band is located between the Ce 4*f* and Ce 5*d* states. The most important differences are in the mid-gap states which have been decomposed by projecting the DOS on each atom, pDOS. Systems with vacancies present a mid-gap state just below the Fermi energy. Both, TiO_2 and CeO_2, are n-type semiconductors so, in principle, vacancies can generate Ti^{3+} or Ce^{3+} atoms. However, as a consequence of a strong oxide-oxide interaction,[48, 49] pDOS clearly demonstrates that this mid-gap state corresponds only to Ce^{3+} for the CeO_x/TiO_2 system or Ce^{3+} and Pt for the $Pt/CeO_x/TiO_2$ system. When the area of the mid-gap state of the CeO_x/TiO_2 system (see blue line in Figure 2 inset) is integrated, we found that the peak represents 2 electrons localized in two different Ce atoms around the vacancy.
When Pt is present on the system, another two Pt 5*d* states appear between the Ce^{3+} mid gap state and the valence band, just below and above -1.0 eV. These Pt 5*d* states seem to be the main reason for the band gap reduction and the absorption in the visible region of the spectra.[16] However, absorption spectra were computed in order to confirm the influence of Pt and the differences between all the hierarchical nanostructures.

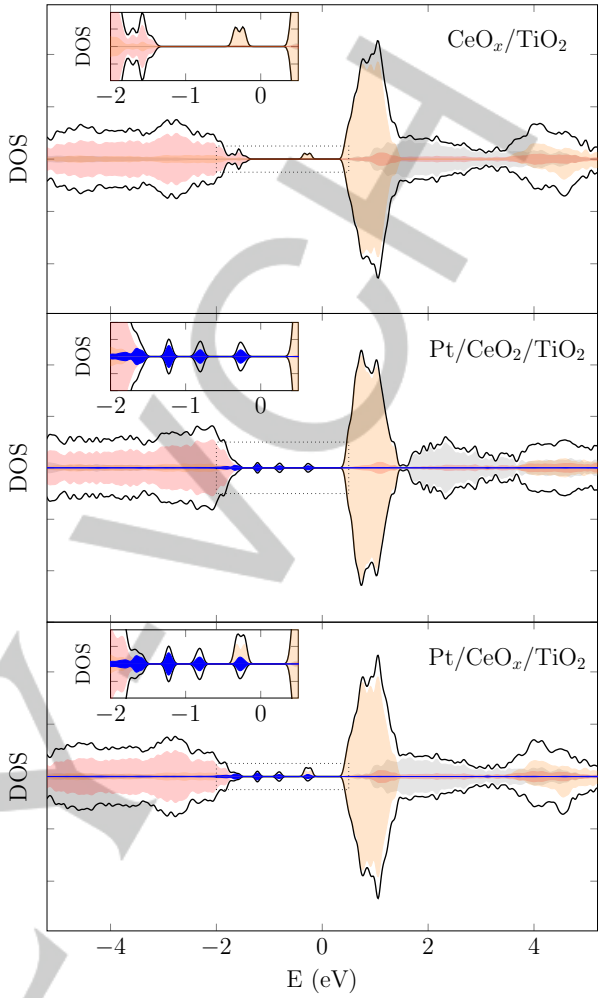

Figure 2. Density of states, DOS, for the 2D system with vacancies, CeO_x/TiO_2 (upper panel), with adsorbed Pt atoms, $Pt/CeO_2/TiO_2$ (middle panel), and with Pt and vacancies, $Pt/CeO_x/TiO_2$ (bottom panel). Inset with the mid-gap states area have been included. Projected density of states color code: O = red; Ce = orange; Ti = grey; Pt = blue.

Optoelectronic properties. Previous studies have not detected significant differences among the absorption spectra of 1D, 2D and 3D hierarchical structures. Thus, our 2D interface model has been selected to simulate the electronic absorption spectra and to compare with the experimental results in order to reduce the computational cost. All the calculated spectra have been shifted to the blue region because of the well-known band gap underestimation by GGA functionals. In this regard, experimental TiO_2 spectra were used as a reference aligning the peaks that correspond to the O 2p – Ti 3d transition by a shift of 0.3 eV (Figure 3a). This shift was applied to all the simulated spectra obtaining good agreement with experimental spectra (Figure 3a). The intensity of all the spectra was also normalized to obtain a straightforward comparison between calculated and reported experimental spectra.[18] The TiO_2/CeO_2 interface spectrum presents features not seen in the spectra of TiO_2 and CeO_2 separately. The edge of the main adsorption band is clearly shifted to lower energies compared to the main bands in TiO_2 and CeO_2. This can be explained by the DOS examined in the previous section. The position of the Ce 4f band at lower energies than the Ti 3d band opens the door to a new O 2p (TiO_2) → Ce 4f

transition. At the same time, the greater number of vacancies at the interfaces creates mid-gap states that are the responsible of the small tail of the band beyond 500 nm (Figure 3a). When Pt is adsorbed, the absorbance in the 500-700 nm region increases (Figure 3b) with respect to the TiO_2/CeO_2 system. The origin of this effect, also observed in the calculated spectra, is the appearance of Pt 5d states in the middle of the gap.

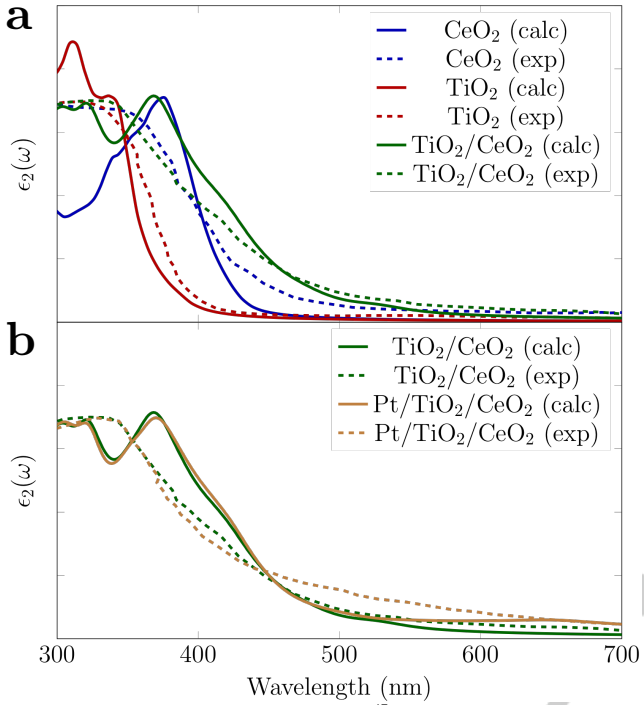

Figure 3. Calculated (solid) and experimental[17] (dashed) absorption spectra for (a) TiO_2 (red), CeO_2 (blue), CeO_x/TiO_2 (green) and (b) $Pt/CeO_x/TiO_2$ (yellow).

Effects of late transition or noble metals. Once the main features and transitions of the adsorption spectra have been analyzed, the validated model can be used for looking for new candidates with potentially similar or higher activity than Pt. A screening was performed to explore and simulate the behavior of other transition metals. It is appropriate to include certain caveats here. The systems must present absorbance at the visible region of the spectra to act as water-splitting photocatalyst, however, their activity is also related to other variables such as the role of mid-gap states as charge recombination centers. We have simulated the adsorption spectra of the TiO_2/CeO_2 interface substituting Pt by Ni, Pd, Cu, Pt and Au (Figure 4). Cu, Ag and Au atoms do not improve the absorbance in the 500-700 nm region with respect to Pt, but among the group 10 metals some promising results appear. The $Ni/CeO_x/TiO_2$ system interface presents an absorption spectrum very similar to the $Pt/CeO_x/TiO_2$, with Ni being considerably cheaper than Pt. Moreover, Pd even increases the absorbance in that region. If the origin of this behavior stemmed from the mid gap states created by the metal adsorption, there should be a connection between the DOS and the absorption spectra of each system. To substantiate such a relationship, the projected DOS of the metals for the different $M/CeO_2/TiO_2$ models were integrated in the mid-gap region (Table S1, Figure S5). Two well-differentiated groups were identified: one constituted by Pd, Ni and Pt and a second one composed by Cu, Ag and Au. The electron integration shows that Pd, Ni and Pt exhibit more electrons in the mid-gap region, explaining the features observed in the simulated electronic spectra.

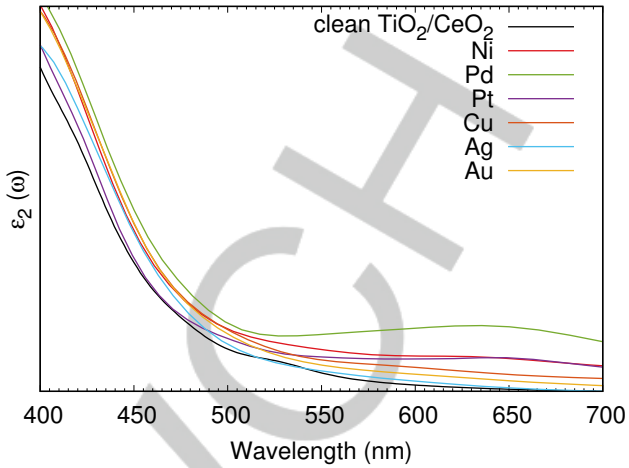

Figure 4 Calculated absorption spectra for $M/CeO_x/TiO_2$ interfaces. Colors: Ni = red, Pd = green, Pt = purple, Cu = orange, Ag = light blue, Au = brown.

Conclusions

The electronic and optoelectronic properties of TiO_2/CeO_2 hierarchical nanostructures and the $Pt/TiO_2/CeO_2$ system have been studied to explain their properties as photocatalyst for the splitting of water in the visible region. Preferential adsorption sites were stablished for 1D, 2D and 3D ceria models and compared with previous literature for clean CeO_2 surfaces, cluster and steps. Pt-oxygen vacancy interaction was analysed to explain the adsorption behaviour of this metal on these models. We found that the relative position of the Ce 4f band explains the shift of the main O 2p-M band in the absorption spectra. Pt mid-gap states are crucial for the optical properties of the system in the visible region. The concordance between experiment and simulations not only explains the behaviour of this system but also open the door to predict the properties of other possible candidates. Promising results have been obtained using Ni and Pd as adsorbed metal at the interface resulting in a higher density of states in the gap and, as a consequence, increased absorption in the visible region.

Computational details and model

Density functional theory (DFT) calculations were performed using the generalized gradient approximation (GGA) exchange correlation functional proposed by Perdew et al.[40] and the projector augmented wave method (PAW)[41,42] as implemented in the Vienna Ab-initio simulation package (VASP) 5.2 code.[41,43,44,45] In all these calculations the electronic states were expanded in a plane-wave basis set with a cutoff energy of 400 eV. DFT+U formalism was used to adequately represent the electronic structure of the 4f states of Ce atoms, especially to localize Ce^{3+} species. The Hubbard U term was included using the rotationally invariant approach proposed by Dudarev et al.,[46] in which the Coulomb U and the exchange J parameters are combined into a single parameter Ueff = U − J. A Ueff of 4.5 eV was used for 4f Ce orbitals which was self-consistently estimated by Fabris et al.[47] using the linear-response described by Cococcioni and de Gironcoli.[48] This Ueff is in the range of values

usually proposed in the literature (4.5−5.5 eV) for CeO_2 and other cerium oxides based materials. [49,50,51,52,53,54] A Ueff parameter of 4.5 eV was selected for the 3d states of Ti atoms to reproduce the experimental values of the gap between the Ce^{3+} 4f and Ti^{3+} 3d levels observed in the valence photoemission spectra of the Ce/TiO_2 (110) system.[19] We have used different ***k***-point meshes depending on the model. While 1D and 3D models were calculated using a 1×1×1 Γ-centered mesh, a 3×3×1 Γ-centered mesh was used for the 2D models. A cutoff of 400 eV was used in all the calculations. As validation test, Pt adsorption energies were calculated with a higher cutoff (500 eV) and denser k-mesh (4×4×1) in the 2D model. The adsorption energies are modified in less than a 3%. Optical spectra were simulated using the imaginary part of the frequency-dependent dielectric function $\varepsilon_2(\omega)$, as proposed by Gajdoš et al.[55]

TiO_2 (110) surface is usually chosen to model rutile TiO_2 surface because of its stability, however, following previous microscopy data, our models are based on CeO_2 particles exhibiting (001) facets that were growth on TiO_2 (112) surface facets.[16, 17] The polar nature of both surfaces, called type 3 according to Tasker classification,[56] was stabilized by reconstruction. In these cases, half of the charges from the top layer were moved to the bottom layer quenching the dipole moment of the slab.[56] As a consequence of the presence of a ceria-titania interface, a net dipole moment still remains after the reconstruction so dipole corrections were added to ensure the convergence of the self-consistent field.[57, 58] To describe the interface between a ceria particle and the titania support, different models were built to study the chains, clusters and nanoparticles experimentally characterized by microscopy.[18] Conventional TiO_2 (-112) lattice vectors a and b were not used but (a+b) and (a-b), [110] and [1-10], directions in order to minimize the misfit of TiO_2-CeO_2 surfaces. This slab is denoted as (√2×√2) R45 TiO_2(−112) in Wood's notation. The 1D nanostructure was modelled using a CeO_2 monomer on top of the TiO_2 surface (Figure 1a and 1b). The 2D nanostructure was modelled growing five or two layers of a (2×2) CeO_2 (001) slab on top of the TiO_2 substrate having a misfit of only 1.7% with respect to the TiO_2 surface (Figure 1c). The 3D nanocluster consists on a $(CeO_2)_{13}$ cluster exposing the (001) and (110) planes. (Figure 1d). Adsorption energies, Eads, were calculated with respect to an isolated Pt atom on a 20×20×20 Å box as $E_{ads} = E_{Pt/surf} - (E_{Pt}+E_{surf})$. Thus, negative adsorption energies represent bound states, stable with respect to desorption.

Acknowledgements

This work was funded by the Ministerio de Economía y Competitividad (Spain, grant CTQ2015-64669-P) and European FEDER. Computational resources were provided by the Barcelona Supercomputing Center/Centro Nacional de Supercomputación (Spain). The work performed at Brookhaven National Laboratory was supported by the U.S. Department of Energy, Office of Science, Office of Basic Energy Sciences, and Catalysis Science Program under contract No. DE-SC0012704. J. J. P. thanks Universidad de Sevilla for the postdoctoral fellowship and European Union's Horizon 2020 research and innovation programme under the Marie Skłodowska Curie grant agreement HT-PHOTO-DB No 752608.

Keywords: TiO_2, CeO_2, interface, Pt, water splitting

[1] S. Wendt, P. T. Sprunger, E. Lira, G. K. H. Madsen, Z. Li, J. Ø. Hansen, J. Matthiesen, A. Blekinge-Rasmussen, E. Lægsgaard, B. Hammer and F. Besenbacher, *Science* **2008**, *320*, 1755-1759.

[2] A. Le Gal, S. Abanades, *J. Phys. Chem. C* **2012**, *116*, 13516-13523.

[3] K. Cheng, W. Sun, H. Y. Jiang, J. Liu, J. Lin. *J. Phys. Chem. C* **2013**, *117*, 14600-14607.

[4] A. Primo, T. Marino, A. Corma, R. Molinari, H. García, *J. Am. Chem. Soc.* **2011**, *133*, 6930-6933.

[5] Y. Zhang, F. Lv, T. Wu, L. Yu, R. Zhang, Bo. Shen, X. Meng, Z. Ye and P. K. Chu *J. Sol-Gel Sci. Technol.* **2011**, ***59***, 387-391.

[6] R. Farra, M. García-Melchor, M. Eichelbaum, M. Hashagen, W. Frandsen, J. Allan, F. Girgsdies, L. Szentmiklósi, N. López and D. Teschner, *ACS Catal*. **2013**, *3*, 2256-2268.

[7] J. J. Plata, J. Graciani, J. Evans, J. A. Rodriguez and J. F. Sanz *ACS Catal*. **2016**, **6**, 4608-4615.

[8] Y. Yu, Y. Zhu and M. Meng. *Dalton Trans*. **2013**, *42*, 12087-12092.

[9] A. M. Marquez, J. J. Plata, Y. Ortega, J. F. Sanz, G. Colon, A. Kubacka, M. Fernandez-Garcia, *J. Phys. Chem. C*, 2012, **116**, 18759-18767.

[10] S. Watanabe, X. Ma and C. Song *J. Phys. Chem. C*, **2009**, *113*, 14249-14257.

[11] A. R. Albuquerque, A. Bruix, I. M. G. dos Santos, J. R. Sambrano and F. Illas *J. Phys. Chem.* C, **2014**, *118*, 9677-9689.

[12] J. B. Park, J. Graciani, J. Evans, D. Stacchiola, S. D. Senanayake, L. Barrio, P. Liu, J. F. Sanz, J. Hrbek and J. A. Rodríguez *J. Am. Chem. Soc*. **2010**, *132*, 356-363.

[13] A. Bruix, J. A. Rodriguez, P. J. Ramírez, S. D. Senanayake, J. Evans, J. B. Park, D. Stacchiola, P. Liu, J. Hrbek and F. Illas *J. Am. Chem. Soc*. **2012**, *134*, 8968-8974.

[14] J. Guo, M. J. Janik and C. Song *J. Phys. Chem. C* **2012**, *116*, 3457-3466.

[15] M. Nolan *J. Chem. Phys*. **2013**, *139*, 184710.

[16] S. Kundu, J. Ciston, S. D. Senanayake, D. A. Arena, E. Fujita, D. Stacchiola, L. Barrio, R. M. Navarro, J. L. G. Fierro and J. A. Rodriguez. *J. Phys. Chem. C* **2012**, *116*, 14062-14070.

[17] A. C. Johnston-Peck, S. D. Senanayake, J. J. Plata, S. Kundu, W. Q. Xu, L. Barrio, J. Graciani, J. F. Sanz, R. M. Navarro, J. L. G Fierro, E. A. Stach and J. A. Rodriguez. *J. Phys. Chem. C* **2013**, *117*, 14463-14471.

[18] S. Luo, T.-D Nguyen-Phan, A. C. Johnston-Peck, L. Barrio, S. Sallis, D. A. Arena, S. Kundu, W. Xu, F. J. Piper, E. A. Stach, D. E. Polyansky, E. Fujita, J. A. Rodriguez and S. D. Senanayake *J. Phys. Chem. C* **2015**, *119*, 2669-2679.

[19] J. B. Park, J. Graciani, J. Evans, D. Stacchiola, S. Ma, P. Liu, A. Nambu, J. F. Sanz, J. Hrbek and J. A. Rodriguez *Proc. Natl. Acad. Sci. U.S.A*. **2009**, *106*, 4975-4980.

[20] S. Agnoli, A. E. Reeder, S. D. Senanayake, J. Hrbek and J. A. Rodríguez, *Nanoscale*, **2014**, *6*, 800-810.

[21] S. Luo, L. Barrio, T. D. Nguyen-Phan, D. Vovchok, A. C. Johnston-Peck, W. Xu, E. A. Stach, J. A. Rodriguez and S. D. Senanayake *J. Phys. Chem. C* **2017**, *121* (12), 6635-6642.

[22] L. Xu, C. Wang, H. Chang, Q. Wu, T. Zhang and J. Li, Environ. Sci. Technol. **2018**, *52*, 7064-7071.

[23] H. Abdullah, M. R. Khan, M. Pudukudy, Z. Yaakob and N. A. Ismail J. Rare Earths **2015**, *33*, 1155-1161.

[24] Y. Wang, J. Zhao, T. Wang, Y. Li, X. Li, J. Yin and C. Wang *J. Catal* **2016**, *337*, 293-302.

[25] T. M. Wandre, P. N. Gaikwad, A. S. Tapase, K. M. Garadkar, S. A. Vanalakar, P. D. Lokhande, R. Sasikala and P. P. Hankare, J. Mater. Sci. Mater. Electron. **2016**, *27*, 825-833.

[26] L. T. T. Tuyen, D. A. Quang, T. T. T. Toan, T. Q. Tung, T. T. Hoa, T. X. Mau and D. Q. Khieu *J. Environ. Chem. Eng.* **2018**, *6*, 5999-6011.
[27] M. J. Munoz-Batista, M. N. Gomez-Cerezo, A. Kubacka, D. Tudela, and M. Fernandez-Garcia *ACS Catal.* **2014**, *4*, 63-72.
[28] M. Muñoz-Batista, M. Ferrer, M. Fernández-García and A. Kubacka, *Appl. Catal. B Environ.* **2014**, *350*, 154–155.
[29] H. Eskandarloo, A. Badiei and M. A. Behnajady *Ind. Eng. Chem. Res.* **2014**, *53*, 7847-7855.
[30] C. Yang, X. Yu, P. N. Pleßow, S. Heißler, P. G. Weidler, A. Nefedov, F. Studt, Y. Wang and C. Wöll *Angew. Chemie - Int. Ed.* **2017**, *56*, 14301-14305.
[31] R. Fiorenza, M. Bellardita, L. Palmisano and S. Scirè, J. Mol. Catal. A Chem. **2016**, *415*, 56-64.
[32] E. T. Kho, S. Jantarang, Z. Zheng, J. Scott and R. Amal *Engineering* **2017**, *3*, 393-401.
[33] S. Li, J. Cai, X. Wu, B. Liu, Q. Chen, Y. Li and F. Zheng *Hazard. Mater.* **2018**, *346*, 52-61.
[34] Z. Yang, Z. Lu and G. Luo *Phys. Rev. B* **2007**, *76*, 075421
[35] A. Bruix, K. M. Neyman and F. Illas J. *Phys. Chem. C* **2010**, *114*, 14202-14207.
[36] G. N. Vayssilov, A. Migani, K. Neyman, *J. Phys. Chem. C* **2011**, *115*, 16081-16086.
[37] D. Ma, T. Li, Q. Wang, G Yang, C. He, B. He, Z. Lu and Z. Yang *Appl. Surf. Sci.* **2017**, *394*, 47-57.
[38] F. Dvorák, F. Camellone, A. Tovt, N.-D Tran, F. R. Negreiros, M. Vorokhta, T. Skála, J. Myslivecek and S. Fabris *Nature Comm.* **2016**, *7*, 10801.
[39] G. N. Vayssiliv, Y. Lykhach, A. Migani, T. Staudt, G. P. Petrova, N. Tsud, T. Skála, A. Bruix, F. Illas, K. C. Prince, V. Matolín, K. Neyman and J. Libuda *Nature Mater.* **2011**, *10*, 310-315.
[40] J. P. Perdew, J. A. Chevary, S. H. Vosko, K. A. Jackson, M. R. Pederson, D. J. Singh and C. Fiolhais *Phys. Rev. B* **1992**, *46*, 6671.
[41] G. Kresse and D. Joubert *Phys. Rev. B.* **1999**, *59*, 1758.
[42] P. Blöchl *Phys. Rev. B*. **1994**, *50*, 17953.
[43] G. Kresse and J. Furthmüller *Phys. Rev. B*. **1996**, *54*, 11169.
[44] G. Kresse and J. Furthmüller *Comput. Mater. Sci.* **1996**, *6*, 15-50.
[45] G. Kresse and J. Hafner *Phys. Rev. B* **1993**, *47*, 558.
[46] S. L. Dudarev, G. A. Botton, S. Y. Savrasov, C. J. Humphreys and A. P. Sutton *Phys. Rev. B* **1998**, *57*, 1505.
[47] S. Fabris, S. de Gironcoli, S. Baroni, G. Vicario and G. Balducci *Phys. Rev. B* **2005**, *72*, 237102.
[48] M. Cococcioni and S. de Gironcoli, S. *Phys. Rev. B* **2005**, *71*, 035105.
[49] C. W. M. Castleton, J. Kullgren and K. Hermansson *J. Chem. Phys.* **2007**, *127*, 244704.
[50] D. A. Andersson, S. I. Simak, B. Johansson, I. A. Abrikosov, and N. V. Skorodumova *Phys. Rev. B* **2007**, *75*, 035109.
[51] M. Nolan, S. C. Parker and G. W. Watson *Surf. Sci.* **2005**, *595*, 223-232.
[52] J. L. F. Da Silva, M. V. Ganduglia-Pirovano, J. Sauer, V. Bayer and G. Kresse *Phys. Rev. B* **2007**, *75*, 045121.
[53] J. J. Plata, A. M. Marquez and J. F. Sanz *J. Chem. Phys.* **2012**, *136*, 041101.
[54] J. Graciani, J. J. Plata, J. F. Sanz, P. Liu and J. A. Rodriguez *J. Chem. Phys.* **2010**, *132*, 104703.
[55] M. Gajdoš, K. Hummer, G. Kresse, J. Furthmüller, F. Bechstedt, *Phys. Rev. B* **2006**, *73*, 045112.
[56] P. W. Tasker *J. Phys. C: Solid State Phys.* **1979**, *12*, 4977-4984.
[57] G. Makov and M. C. Payne *Phys. Rev. B* **1995**, *51*, 4014.
[58] J. Neugebauer and M. Scheffler *Phys. Rev. B* **1992**, *46*, 16067.

ARTICLE

Interfaces and Pt: Ceria-titania interfaces play a crucial role in different chemical processes but are especially promising for the photocatalytic splitting of water in the visible region when Pt is added to the system. In this article, the structural, electronic and optoelectronic properties of $Pt/CeO_2/TiO_2$ systems containing 1D, 2D, and 3D ceria particles are analyzed by means of density functional calculations.

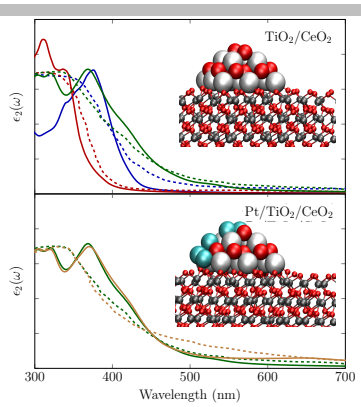

Jose J. Plata, Elena R. Remesal, Jesús Graciani, Antonio M. Márquez, José A. Rodríguez, and Javier Fernández Sanz**

Page No. – Page No.

Understanding the photocatalytic properties of the Pt/CeOx/TiO_2 systems: structural effects on the electronic and optic properties